processes

MDPI

Article

Multivariate Parameter Determination of Multi-Component Isotherms for Chromatography Digital Twins

Steffen Zobel-Roos [1], Florian Vetter [1], Daniel Scheps [2], Marcus Pfeiffer [2], Matthias Gunne [3], Oliver Boscheinen [2] and Jochen Strube [1,*]

[1] Institute for Separation and Process Technology, Clausthal University of Technology, Leibnizstraße 15, D-38678 Clausthal-Zellerfeld, Germany
[2] CMC Microbial Platform, Sanofi-Aventis Deutschland GmbH, D-65926 Frankfurt am Main, Germany
[3] IA MSAT M&I DS, Sanofi-Aventis Deutschland GmbH, D-65926 Frankfurt am Main, Germany
* Correspondence: strube@itv.tu-clausthal.de; Tel.: +49-5323-722-355

Abstract: Many fundamental decisions in the process design of a separation task are conducted in an early stage where, unfortunately, process simulation does not have the highest priority. Subsequently, during the setup of the digital twin, dedicated experiments are carried out in the design space that was established earlier. These experiments are most often too complicated to conduct directly. This paper addresses the idea of a combined approach. The early-stage buffer screening and optimization experiments were planned with the Design of Experiments, carried out and then analyzed statistically to extract not only the best buffer composition but also the crucial model parameters, in this case the isotherm dependency on the buffer composition. This allowed the digital twin to predict the best buffer composition, and if the model-predicted control was applied to keep the process at the optimal productivity at a predetermined purity. The methodology was tested with an industrial peptide purification step.

Keywords: peptide purification; isotherm determination; design of experiments

Citation: Zobel-Roos, S.; Vetter, F.; Scheps, D.; Pfeiffer, M.; Gunne, M.; Boscheinen, O.; Strube, J. Multivariate Parameter Determination of Multi-Component Isotherms for Chromatography Digital Twins. *Processes* **2023**, *11*, 1480. https://doi.org/10.3390/pr11051480

Academic Editors: Alina Pyka-Pająk, Piotr Rybarczyk, Adina Magdalena Musuc and Roberto Pisano

Received: 22 February 2023
Revised: 5 May 2023
Accepted: 11 May 2023
Published: 12 May 2023

1. Introduction

Chromatography is a widely used unit operation in chemical and pharmaceutical engineering with broad fields of application from low-cost bulk chemicals to high potential pharmaceuticals. Because of the variety of potential chromatography processes such as batch chromatography or various continuous process options, process modelling has been state of the art for decades [1–6]. With increasing computational power, model parameter determination has become the bottleneck for fast and efficient model implementation. There is an increasing number of different approaches that can, in general, be separated into two categories.

One approach is to measure each model parameter individually, preferably decoupled from the other effects. Fluid dynamics, e.g., the axial dispersion coefficients measured with tracer experiments [3,7–9]; thermodynamics, e.g., isotherms measured with dedicated experiments such as shaking flask experiments, frontal analysis or perturbation [1,10,11]; and mass transfer are evaluated separately. Although delivering precise and accurate results, this approach is time consuming.

The other approach is obtaining parameters from simple experiments, ideally directly from chromatograms. This is possible with fitting routines [12–14], neuronal networks [15–17] or alike. This is a fast approach; the resulting quality, however, might not be the best, especially if two parameters can describe the same effect. Peak shape, for example, is influenced by fluid dynamics, thermodynamics and mass transfer. Of course, a combined approach is also possible.

Great efforts have been devoted to the development of different isotherm models and the corresponding parameter determination methods, especially for gradient separations. In most cases, the thermodynamic behaviour of the analytes/compounds is only investigated for the modifier. In some cases, isotherms are determined for two different parameters, such as the pH and ionic strength. This was obviously needed for mixed-mode chromatography [18–21] but was also undertaken for other media [22,23]. The determination of isotherm dependency for more buffer components is rarely undertaken since the experimental effort increases exponentially. Nevertheless, most buffer components do have a significant influence on retention behaviour. In most cases, however, the buffer composition is examined in an early process stage and is kept untouched later. Often, only the gradient gets optimized and modelled thoroughly. Fluctuations in the buffer composition are, therefore, often not representable in chromatography models.

For this case study, a reversed-phase polishing step for an industrial peptide production was investigated. To evaluate the influences of buffer composition, a Design of Experiments approach was taken. Three components, counter ion, stabilizer and the pH value were investigated. The DoE was performed with downscaled preparative chromatography runs and first analysed for the significance of each parameter. The preparative DoE runs were further evaluated to obtain the model parameters to describe the isotherm dependency on each buffer compound.

2. Modelling Chromatography: General Rate Model

The chromatography model used throughout this work, namely the general rate model, as well as the general modelling approach, is described in detail in Zobel-Roos et al. [24]. The model was used and parametrized in Zobel-Roos et al. [25].

In order for the model to become a digital twin, it was necessary for the real process to provide information back to the model. In this case, this was accomplished through the use of Process Analytical Technologies (PAT) tools that converted the Diode Array Detector (DAD) signals to product and impurity concentrations in-line and in real time [26,27]. Furthermore, neural networks are sometimes used to determine or adjust model parameters during the operation, such as the fluid dynamic parameters [15]. The coupling with the process control system was described by the authors in [28,29].

The general rate model can be separated into three parts: the mass balance for the mobile phase, the mass balance for the light phase and the description of the equilibrium. The authors of [1,2,5,30–32] provide more detail regarding derivation, assumptions and further information.

Mass balance of mobile phase:

The mass balance of the mobile phase consists of four terms reading from left to right: storage, convective flow, axial dispersion and mass transport [1]:

$$\frac{\partial c_i}{\partial t} = -u_{int} \cdot \frac{\partial c_i}{\partial x} + D_{ax} \cdot \frac{\partial^2 c_i}{\partial x^2} - \frac{6}{d_p} \cdot \frac{(1-\varepsilon_s)}{\varepsilon_s} \cdot k_{f,i} \cdot \left(c_i - c_{p,i}\big|_{r=R_p} \right) \quad (1)$$

with u_{int} as interstitial velocity, D_{ax} as axial dispersion coefficient, ε_s as voidage, d_p as particle diameter and $k_{f,i}$ as film mass transport coefficient. The use of film mass transport coefficient demands the consideration of pore diffusion in the mass balance of the stationary phase. However, film mass transport and pore diffusion can be combined, resulting in the lumped pore diffusion model [32]. Here, the film mass transport coefficient $k_{f,i}$ was replaced with an effective mass transport coefficient k_{eff}. This simplification is often applied in the early process development to reduce the model parameter determination efforts at the expense of the model accuracy and process understanding. An even further simplification is the lumped kinetic model that neglects the intraparticle pores completely [32].

Mass balance of stationary phase:

The mass balance of the stationary phase is mostly dominated by pore diffusion $D_{p,i}$ and surface diffusion $D_{S,i}$ [30,33]:

$$\varepsilon_{p,i} \cdot \frac{\partial c_{p,i}}{\partial t} + (1 - \varepsilon_{p,i}) \cdot \frac{\partial q_i}{\partial t} = \frac{1}{r^2} \frac{\partial}{\partial} \left[r^2 \left(\varepsilon_{p,i} \cdot D_{p,i} \cdot \frac{\partial c_{p,i}}{\partial r} + (1 - \varepsilon_{p,i}) \cdot D_{S,i} \frac{\partial q_i^*}{\partial r} \right) \right] \quad (2)$$

with $c_{p,i}$ as the concentration of component i within the pores and q_i as the surface loading of component i. For larger molecules, surface diffusion is often neglected or combined with pore diffusion into one effective diffusion coefficient D_{eff} [10,33].

$$D_{eff,i} = \varepsilon_{p,i} \cdot D_{p,i} + (1 - \varepsilon_p, i) \cdot D_{S,i} \frac{\partial q_i^*}{\partial c_{p,i}} \quad (3)$$

Combining Equations (2) and (3) results in:

$$\varepsilon_{p,i} \cdot \frac{\partial c_{p,i}}{\partial t} + (1 - \varepsilon_{p,i}) \cdot \frac{\partial q_i}{\partial t} = D_{eff,i} \left(\frac{\partial^2 c_{p,i}}{\partial r^2} + \frac{2}{r} \cdot \frac{\partial c_p}{\partial r} \right) \quad (4)$$

For the lumped pore diffusion model, the mass balance for the stationary phase reads [32]:

$$\varepsilon_{p,i} \cdot \frac{\partial c_{p,i}}{\partial t} + (1 - \varepsilon_{p,i}) \cdot \frac{\partial q_i}{\partial t} = \frac{6}{d_p} \cdot \frac{(1 - \varepsilon_s)}{\varepsilon_s} \cdot k_{f,i} \cdot (c_i - c_{p,i}|) \quad (5)$$

Adsorption equilibrium:

There is a vast number of approaches to describe the adsorption equilibrium, mostly depending on the adsorption mechanism and mode of operation [11,34–45]. For this simulation study, competitive Langmuir isotherms were used [10,46]:

$$q_i = \frac{q_{max,i} \cdot K_i \cdot c_i}{1 + \sum_{j=1}^{n} K_j \cdot c_j} \quad (6)$$

Here, K_i is the Langmuir coefficient and $q_{max,i}$ the maximum loading capacity of component i. There are different notations found in the literature, e.g., with the use of the Henry coefficient H_i. All notations can be transferred into the other with:

$$H_i = q_{max,i} \cdot K_i \quad (7)$$

All necessary parameters for fluid dynamic (D_{ax}, ε_s and $\varepsilon_{p,i}$), mass transfer ($k_{f,i}$) and adsorption equilibrium were measured in a previous work [25]. The Langmuir isotherm was measured for the modifier, a short-chain aliphatic alcohol.

3. Materials and Methods

3.1. Feed, Buffer Components and Columns

The feed solution was taken from an industrial peptide process. The short-chain aliphatic alcohol, buffer salts and stabilisers were obtained in pharmaceutical production quality from Sanofi-Aventis Deutschland GmbH. Short-chain aliphatic alcohol was taken from the production process.

Preparative chromatography was performed with silica-based reversed-phase media in self-packed glass columns (Götec-Labortechnik GmbH, Bickenbach, Germany). Analytical chromatography was performed with a RP-18 column.

3.2. Preparative Chromatography

All preparative runs were performed with the same method. Each run started with 1 column volume (CV) equilibration followed by 14 CV loading. The gradient was started directly afterwards. A run was terminated with a regeneration step after the elution of the main peak, detected via UV–Vis at 280 nm.

3.3. Software

For process simulation and isotherm parameter fitting, Aspen Custom Modeler (Aspentech, Bedford, MA, USA) was used. The Design of Experiments plan was set up and evaluated with JMP (SAS Institute, Cary, NC, USA). JMP was also used to statistically evaluate the isotherm parameters using multiple linear regression.

4. Design of Experiments

To identify the significance of each parameter in the given range, the following was used:

- Counter ion: 25–100 mM;
- Buffer: 50–150 mM;
- pH: 3.35–3.7.

A three-factor, level two, full factorial Design of Experiments plan was carried out. It included one centre point with three repetitions to evaluate the reproducibility. The boundaries were conceived from prior knowledge. The pattern introduced in Table 1 is used throughout the article to identify the experiments. The centre point is 000 and + and— indicate that the factor is at minimum or maximum. The order of the symbols represents the order as given in Table 1: first, the counter ion; second, the buffer; and third, the pH. Although Table 1 shows the entries in order, the experiments were randomized. Each run was fractionated in 30 s intervals and analysed offline for the target and side component concentrations. The product was pooled out of these fractions to surpass 99% purity. The target values were productivity and yield, normalized to the mean value of the three centre points. The experimental data and results are given in Table 1:

Table 1. Design of Experiments plan.

	Factors			Target Values	
Pattern	CI [mM]	Buffer [mM]	pH [-]	Normalized Yield [-]	Normalized Productivity [-]
(000)	62.5	100	3.53	1.01	1.00
(000)	62.5	100	3.53	0.99	0.99
(000)	62.5	100	3.53	1.00	1.00
(—)	25	50	3.35	0.73	0.61
(–+)	25	50	3.7	1.06	1.08
(-+-)	25	150	3.35	1.09	1.08
(-++)	25	150	3.7	0.93	1.02
(+–)	100	50	3.35	0.93	0.91
(+-+)	100	50	3.7	1.20	1.20
(++-)	100	150	3.35	1.23	1.22
(+++)	100	150	3.7	0.97	0.99

The pareto charts of the standardized effects, given in Figure 1, indicated that each single parameter and each parameter combination had a significant effect on both the yield and productivity. Obviously, a higher yield automatically resulted in a higher productivity. In addition, the changes in the buffer composition had an influence on the retention time as well (see also Figure 4). Therefore, productivity was more affected by the buffer composition.

The results showed that each parameter individually had a positive influence on the target values. Increasing these would increase the outcome. The parameter combinations, however, had a negative impact, especially the combination of the pH and buffer, which had the highest impact values. Although the absolute values given in the pareto charts did not necessarily give the correct ranking or strength of impact, one might assume that the best buffer composition would be:

- A high counter ion (CI) value; and
- A high pH value at a low buffer concentration; or

- A low pH value at a high buffer concentration.

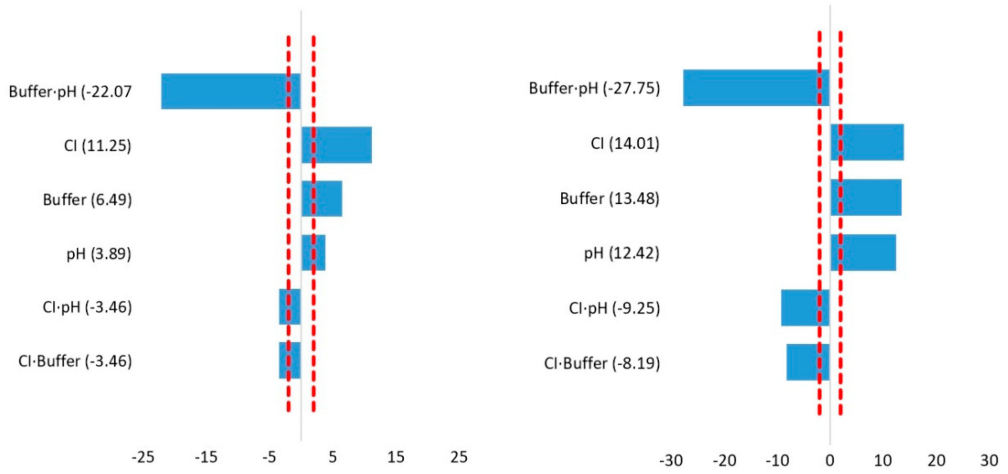

(**a**) Yield (**b**) Productivity

Figure 1. Pareto charts of the standardized effects for (**a**) yield and (**b**) productivity.

The achieved quality of the DoE results was excellent. Figure 2 shows the plots of the measured over the predicted values. All the data points were well on or very close to the red line, indicating that there was a good correlation between the measured and predicted values. This was underlined by very narrow confidence intervals. The other evaluation metrics were also very good. The *p*-values were very low. Generally speaking, the *p*-values describe the accordance of the dataset with a potential explanation, such as that the null-hypothesis is true. Here, the *p*-values were with $p \leq 0.001$ far below the significance boundary of $p = 0.05$ chosen for this DoE. The R^2, here RSq, is near 1 and the Root Mean Square Errors (RMSE) were below 1.5%.

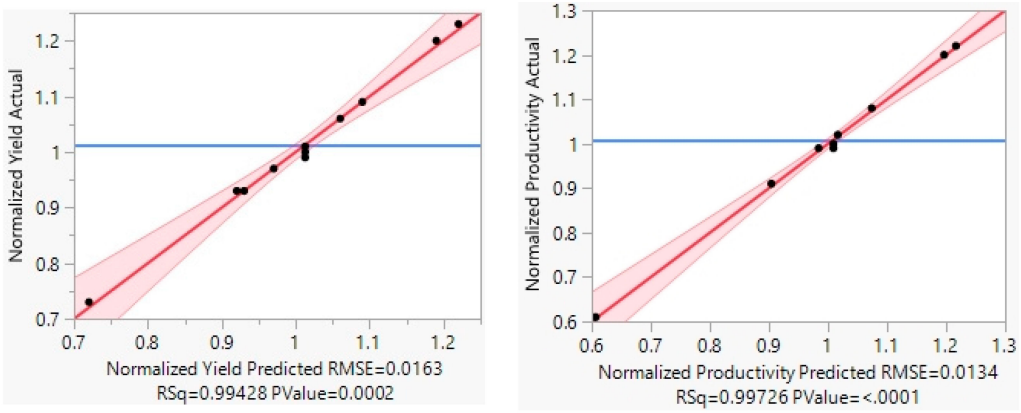

(**a**) Yield (**b**) Productivity

Figure 2. Observed vs. Predicted plots for (**a**) yield and (**b**) productivity.

5. Parameter Extraction

The good results of the DoE, especially the very narrow confidence intervals, indicated that there might be a linear correlation between each individual buffer component and the adsorption isotherm. Figure 1 also suggests that there were interactions between the two buffer parameters. It is worth noting that this assumption can only be made within the observed DoE design space. An extrapolation outside the measured parameter range is in general not recommended by statistic fundamentals.

In previous work [25], the isotherm dependency on the modifier concentration was implemented with 4 factors for each component, $a_{1,i}$, $a_{2,1}$, $b_{1,i}$ and $b_{2,i}$. These factors influence the Langmuir parameters Henry coefficient H_i and maximum loading capacity $q_{max,I}$ depending on the modifier concentration:

$$H_i = a_{1,i} \cdot {c_p}^{a_{2,1}} \tag{8}$$

$$q_{max,i} = b_{1,i} + b_{2,i} \cdot c_p \tag{9}$$

Note that c_p is the concentration of the modifier inside the pores. For clarity, the correct indices for c_p were left out here. In case of linear dependencies between the single buffer compounds and the adsorption equilibrium as well as the two parameter interactions, the four factors mentioned above can be described with an equation such as:

$$y = i_0 + i_1x_1 + i_2x_2 + i_3x_3 + i_{12}x_1x_2 + i_{13}x_1x_3 + i_{23}x_2x_3 \tag{10}$$

where y is one of the four factors, x_i is the concentration of the buffer component and i_i is the component dependent linear factor. The latter should be determinable directly with JMP. To do so, $a_{1,i}$, $a_{2,i}$, $b_{1,i}$ and $b_{2,i}$ were added as new target values to the DoE. The factors themselves were obtained by fitting the simulation results to the experimental chromatograms. Again, the linear correlations looked very good. The *p*-values were between 0.003 and 0.0009, R^2 was above 0.98 and the Root Mean Square Errors were also very low. All the values can be found in Table 2. The observed vs. predicted plots are given in Figure 3, exemplified with b1 and b2. Again, the confidence intervals were narrow. An interesting observation can be undertaken for data point (—). Despite being on the line with the others, it is relatively far outside.

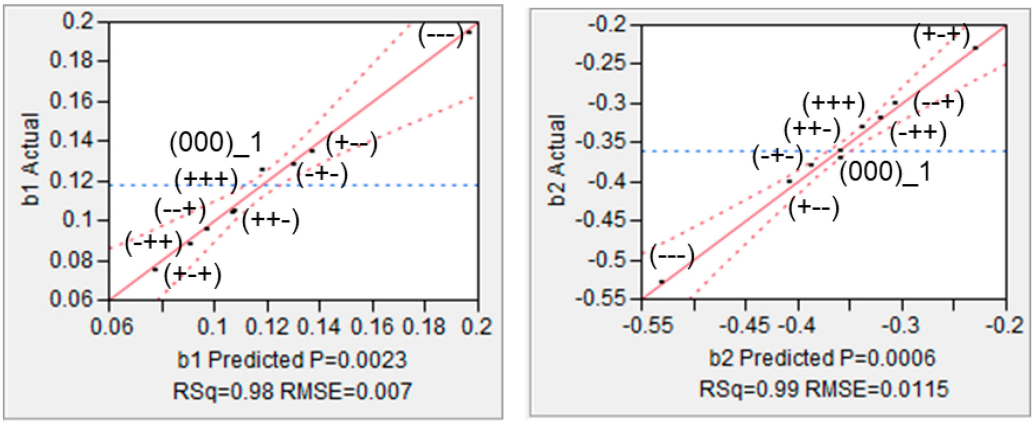

(**a**) b1 (**b**) b2

Figure 3. Observed vs. Predicted plots for the factors (**a**) b1 and (**b**) b2 for the target component.

Table 2. Evaluation metrics for the DoE parameter determination.

	p	R^2	RMSE
a1	0.003	0.98	2.8×10^{-7}
a2	0.0009	0.99	0.0494
b1	0.0023	0.98	0.007
b2	0.0006	0.99	0.0115

6. Discussion

So far, the method was straight forward. The Design of Experiments plan that was set up to determine the dependence of the preparative chromatography runs on the buffer composition was extended by a few isotherm parameters and evaluated statistically to

identify the correlations between these parameters and the buffer composition. Statistically, the results were excellent. The important part, however, was the implementation into the digital twin and that the simulations carried out with different buffer compositions matched the corresponding DoE experiments. In terms of implementation, Equation (10) was added to the model for each isotherm parameter ($a_{1,i}$, $a_{2,i}$, $b_{1,i}$ and $b_{2,i}$).

A comparison between the measured and simulated chromatograms can be found in Figure 4. It can be seen that the digital twin covered the changes in the buffer composition very well. The R^2 values were between 0.858 and 0.998 with an average of 0.952. More importantly, the yield and productivity could be described with good accuracy. On average, the deviation for the yield was 3.6% and the deviation for the productivity was 2.76%. All the values are listed in Table 3.

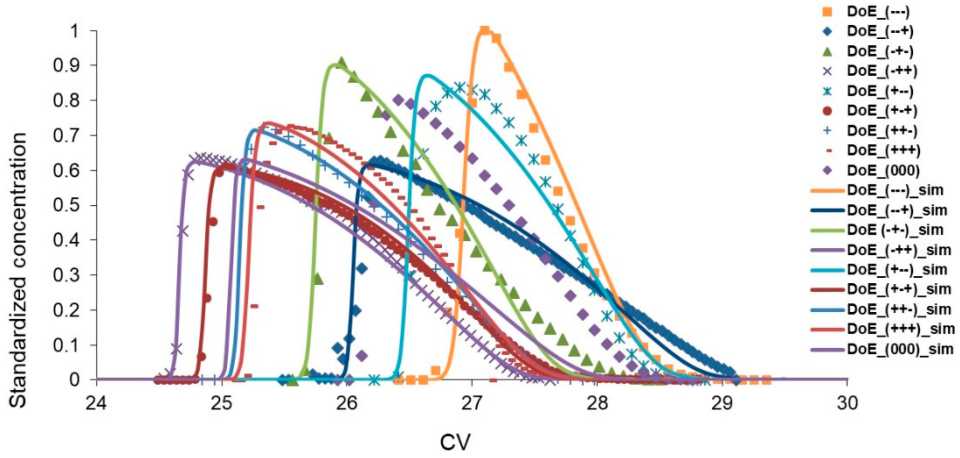

Figure 4. Comparison between DoE experiments (dots) and digital twin simulations (solid lines).

Table 3. Comparison between yield and productivity values for simulations and preparative runs.

Pattern	Simulation		Experiment		Deviation	
	Normalized Yield	Normalized Productivity	Normalized Yield	Normalized Productivity	Yield	Productivity
	[-]	[-]	[-]	[-]	[%]	[%]
(000)_1	1.00	1.00	1.11	1.08	9.88	7.32
(000)_2	1.00	1.00	1.09	1.07	8.65	6.70
(000)_3	1.00	1.00	1.10	1.08	9.12	7.59
(−+)	1.24	1.23	1.17	1.16	−5.51	−5.60
(-+-)	1.22	1.21	1.20	1.16	−1.74	−4.52
(-++)	1.01	1.04	1.03	1.10	1.66	5.03
(+−)	1.00	0.98	1.03	0.98	2.59	−0.19
(+-+)	1.29	1.27	1.32	1.29	1.91	1.81
(++-)	1.28	1.26	1.35	1.32	5.11	4.23
(+++)	1.02	1.03	1.06	1.07	3.89	3.26

Of course, the digital twin could be used to optimize the buffer composition. Contour plots are shown in Figure 5. The top two rows show the values for the buffer and counter ion (top) and the pH over counter ion (middle). In accordance with the pareto charts (Figure 1), the trend for all the components was the more the better. For the combination of the pH and the buffer (bottom), however, the ideal spots are on the two end points, being high pH with a low buffer concentration or a high buffer concentration with low pH. Again, this opposing trend was predicted by the pareto charts. Optimization studies showed that the best result was reached for the combination of the high buffer concentration at low pH. Thus, the best composition was 100 mM counter ion and 150 mM buffer at pH 3.35. This increased the yield by 29% and the productivity by 27% compared to the center point.

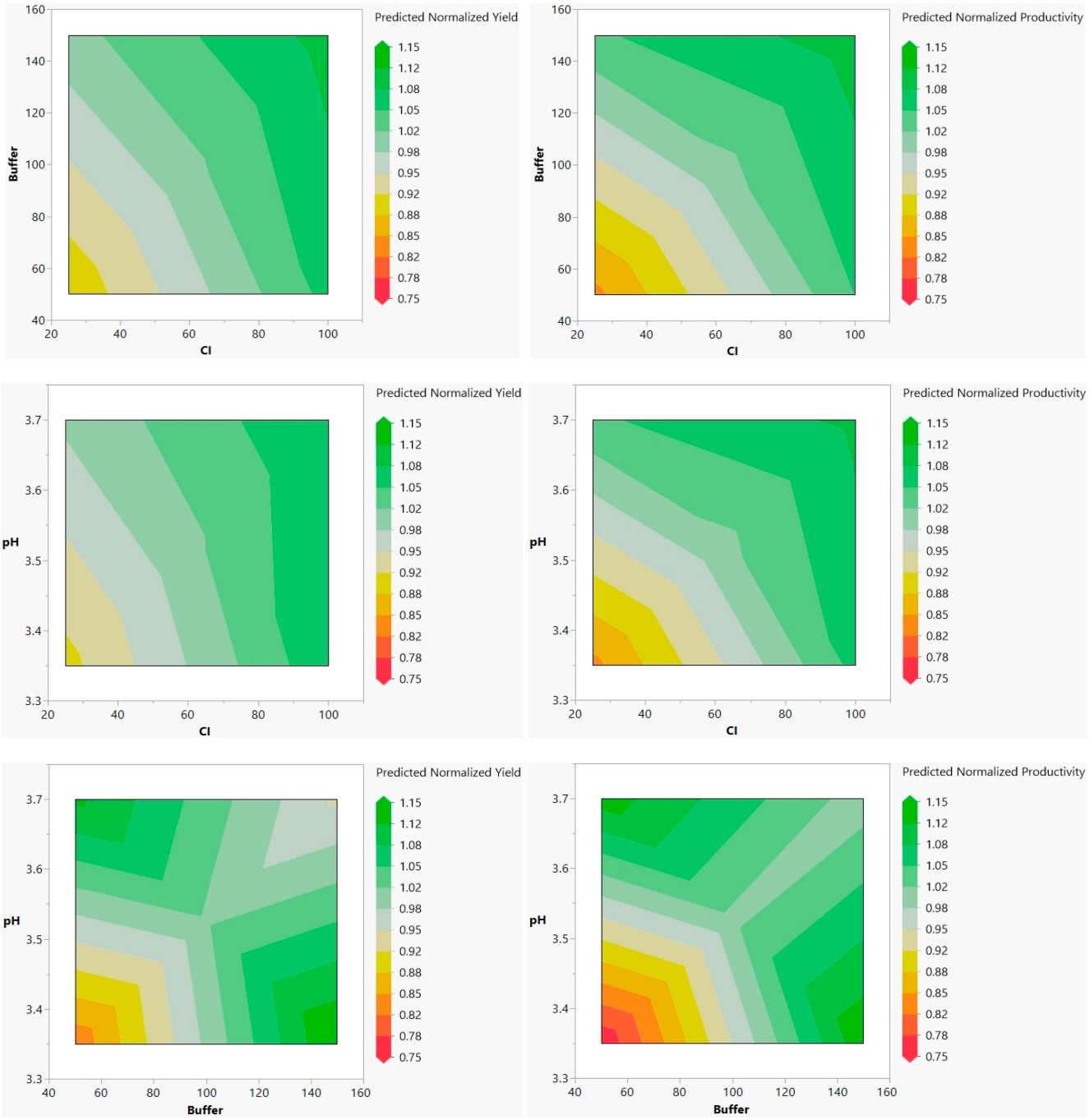

Figure 5. Contour plots showing the influence of two factors on target values, normalized yield on the left and normalized productivity on the right. Top row: Buffer over counter ion, middle row: pH over counter ion, bottom row: pH over buffer. Due to the stepwise change in color instead of a steady color gradient, there were rounding errors leading to the display of more inflection points.

7. Conclusions

Design of experiment plans to estimate the best buffer composition are state of the art as part of the early process development phase, as they are easy to set up and fast to execute. The DoE itself shows the dependency of the performance values on the buffer composition. If coupled with a digital twin, additional information can be extracted easily. In this work, it was shown that fitting the isotherm parameters to the DoE runs and feeding these values back into the DoE as target values generated good correlations. These can

again be integrated into the digital twin, which was able to optimize the buffer composition. This provided an increase in yield of 29% and productivity of 27%.

Additionally, if used for advanced process control, the digital twin is now able to detect fluctuations in the buffer composition and optimize the system, especially the cut points, to maintain the purity at maximum performance.

Author Contributions: Conceptualization, S.Z.-R., F.V., J.S., D.S., M.G. and O.B..; methodology, S.Z.-R. and F.V.; experiments: S.Z.-R., F.V. and M.P. validation, S.Z.-R., F.V., D.S., M.G. and O.B.; writing—original draft preparation, S.Z.-R.; writing—review and editing, J.S., D.S. and M.G. supervision, O.B. and J.S. All authors have read and agreed to the published version of the manuscript.

Funding: We acknowledge support by Open Access Publishing Fund of Clausthal University of Technology.

Institutional Review Board Statement: Not applicable.

Informed Consent Statement: Not applicable.

Data Availability Statement: Data sharing is not applicable to this article.

Conflicts of Interest: Daniel Scheps, Marcus Pfeiffer, Matthias Gunne, and Oliver Boscheinen are Sanofi employees and may hold shares and/or stock options in the company. The further authors declare no conflict of interest.

Abbreviations

c_i	(g/L)	Concentration of component *i*
$c_{p,i}$	(g/L)	Concentration of component *i* inside the pores
CTCC		Continuous Twin Column Chromatography
CV		Column Volume
D_{ax}	(cm^2/s)	Axial dispersion coefficient
D_{eff}	(cm^2/s)	Effective diffusion coefficient
$D_{m,i}$	(cm^2/s)	Molecular diffusion coefficient
d_p	(cm)	Particle diameter
$D_{p,i}$	(cm^2/s)	Pore diffusion coefficient
$D_{S,i}$	(cm^2/s)	Surface diffusion coefficient
DoE		Design of Experiments
$\varepsilon_{p,i}$	(-)	Porosity
ε_s	(-)	Voidage
H_i	(-)	Henry coefficient of component *i*
K_i	(l/g)	Langmuir coefficient of component *i*
k_{eff}	(cm/s)	Effective mass transport coefficient
k_f	(cm/s)	Mass transport coefficient
l	(cm)	Length
MCSGP		Multicolumn Countercurrent Solvent Gradient Purification
PAT		Process Analytical Technology
Pe_i	(-)	Peclet-Number
q_i	(g/L)	Loading of component *i*
$q_{max,i}$	(g/L)	Maximum loading capacity of component *i*
r	(cm)	Radius
Re	(-)	Reynolds-Number
RMSE		Root Mean Square Error
R_p	(cm)	Particle Radius
Sh_i	(-)	Sherwood-Number
t	(s); (min)	Time
$\overline{t_i}$	(s); (min)	Mean residence time
u_{int}	(cm/s)	Interstitial velocity
v	(cm/s)	Velocity
$\dot{V}$	(mL/min)	Volumetric flow
V_{column}	(mL)	Volume of column

η	(mg/cm $*$ s)	Dynamic viscosity
ρ	(g/L)	Density
σ^2	(s^2)	Variance

References

1. Guiochon, G.; Felinger, A.; Shirazi, D.G.; Katti, A.M. *Fundamentals of Preparative and Nonlinear Chromatography*, 2nd ed.; Elsevier Academic Press: Amsterdam, The Netherlands, 2006.
2. Strube, J. *Technische Chromatographie: Auslegung, Optimierung, Betrieb und Wirtschaftlichkeit*; Habil.-Schr. Universität Dortmund, Als Ms. gedr; Shaker: Aachen, Germany, 1999; ISBN 3826568974.
3. Altenhöner, U.; Meurer, M.; Strube, J.; Schmidt-Traub, H. Parameter estimation for the simulation of liquid chromatography. *J. Chromatogr. A* **1997**, *769*, 59–69. [CrossRef]
4. Felinger, A. (Ed.) 3 Models of chromatography. In *Data Analysis and Signal Processing in Chromatography*; Elsevier: Amsterdam, The Netherlands, 1998; pp. 43–78, ISBN 9780444820662.
5. Zobel-Roos, S. *Entwicklung, Modellierung und Validierung von Integrierten Kontinuierlichen Gegenstrom-Chromatographie-Prozessen*; Shaker: Herzogenrath, Germany, 2018; ISBN 3844061878.
6. Seidel-Morgenstern, A. Modeling of Chromatographic Processes. In *Preparative Chromatography*, 3rd ed.; Schmidt-Traub, H., Schulte, M., Seidel-Morgenstern, A., Eds.; WILEY-VCH: Weinheim, Germany, 2020; pp. 311–354, ISBN 9783527344864.
7. Levenspiel, O. *Chemical Reaction Engineering*, 3rd ed.; Wiley: New York, NY, USA, 1999; ISBN 9780471254249.
8. Hejtmánek, V.; Schneider, P. Axial dispersion under liquid-chromatography conditions. *Chem. Eng. Sci.* **1993**, *48*, 1163–1168. [CrossRef]
9. Tallarek, U.; Albert, K.; Bayer, E. Measurement of transverse and axial apparent dispersion coefficients in packed beds. *AIChE J.* **1996**, *42*, 3041–3054. [CrossRef]
10. Carta, G.; Jungbauer, A. *Protein Chromatography: Process Development and Scale-Up*; WILEY-VCH: Weinheim, Germany, 2010; ISBN 978-3-527-31819-3.
11. Seidel-Morgenstern, A. Experimental determination of single solute and competitive adsorption isotherms. *J. Chromatogr. A* **2004**, *1037*, 255–272. [CrossRef] [PubMed]
12. Hahn, T.; Huuk, T.; Heuveline, V.; Hubbuch, J. Simulating and Optimizing Preparative Protein Chromatography with ChromX. *J. Chem. Educ.* **2015**, *92*, 1497–1502. [CrossRef]
13. Osberghaus, A.; Hepbildikler, S.; Nath, S.; Haindl, M.; von Lieres, E.; Hubbuch, J. Determination of parameters for the steric mass action model—A comparison between two approaches. *J. Chromatogr. A* **2012**, *1233*, 54–65. [CrossRef]
14. Huuk, T.C.; Hahn, T.; Osberghaus, A.; Hubbuch, J. Model-based integrated optimization and evaluation of a multi-step ion exchange chromatography. *Sep. Purif. Technol.* **2014**, *136*, 207–222. [CrossRef]
15. Mouellef, M.; Vetter, F.L.; Zobel-Roos, S.; Strube, J. Fast and Versatile Chromatography Process Design and Operation Optimization with the Aid of Artificial Intelligence. *Processes* **2021**, *9*, 2121. [CrossRef]
16. Wang, G.; Briskot, T.; Hahn, T.; Baumann, P.; Hubbuch, J. Estimation of adsorption isotherm and mass transfer parameters in protein chromatography using artificial neural networks. *J. Chromatogr. A* **2017**, *1487*, 211–217. [CrossRef]
17. Gao, W.; Engell, S. Neural Network-Based Identification of Nonlinear Adsorption Isotherms. *IFAC Proc. Vol.* **2004**, *37*, 721–726. [CrossRef]
18. Kreusser, J.; Jirasek, F.; Hasse, H. Influence of pH value and salts on the adsorption of lysozyme in mixed-mode chromatography. *Eng. Life Sci.* **2021**, *21*, 753–768. [CrossRef]
19. Zhu, M.; Carta, G. Protein adsorption equilibrium and kinetics in multimodal cation exchange resins. *Adsorption* **2016**, *22*, 165–179. [CrossRef]
20. Schmidt, A.; Zobel-Roos, S.; Helgers, H.; Lohmann, L.; Vetter, F.; Jensch, C.; Juckers, A.; Strube, J. Digital Twins for Continuous Biologics Manufacturing. In *Process Control, Intensification, and Digitalisation in Continuous Biomanufacturing*; Subramanian, G., Ed.; Wiley: Hoboken, NJ, USA, 2022; pp. 265–350, ISBN 9783527347698.
21. Vetter, F.L.; Zobel-Roos, S.; Mota, J.P.B.; Nilsson, B.; Schmidt, A.; Strube, J. Toward Autonomous Production of mRNA-Therapeutics in the Light of Advanced Process Control and Traditional Control Strategies for Chromatography. *Processes* **2022**, *10*, 1868. [CrossRef]
22. Baumann, P.; Huuk, T.; Hahn, T.; Osberghaus, A.; Hubbuch, J. Deconvolution of high-throughput multicomponent isotherms using multivariate data analysis of protein spectra. *Eng. Life Sci.* **2016**, *16*, 194–201. [CrossRef]
23. Field, N.; Konstantinidis, S.; Velayudhan, A. High-throughput investigation of single and binary protein adsorption isotherms in anion exchange chromatography employing multivariate analysis. *J. Chromatogr. A* **2017**, *1510*, 13–24. [CrossRef]
24. Zobel-Roos, S.; Mouellef, M.; Ditz, R.; Strube, J. Distinct and Quantitative Validation Method for Predictive Process Modelling in Preparative Chromatography of Synthetic and Bio-Based Feed Mixtures Following a Quality-by-Design (QbD) Approach. *Processes* **2019**, *7*, 580. [CrossRef]
25. Zobel-Roos, S.; Vetter, F.L.; Scheps, D.; Pfeiffer, M.; Gunne, M.; Boscheinen, O.; Strube, J. Digital Twin Based Design and Experimental Validation of a Continuous Peptide Polishing Step. *Processes* **2023**, *11*, 1401. [CrossRef]

26. Zobel-Roos, S.; Mouellef, M.; Siemers, C.; Strube, J. Process Analytical Approach towards Quality Controlled Process Automation for the Downstream of Protein Mixtures by Inline Concentration Measurements Based on Ultraviolet/Visible Light (UV/VIS) Spectral Analysis. *Antibodies* **2017**, *6*, 24. [CrossRef]
27. Vetter, F.L.; Zobel-Roos, S.; Strube, J. PAT for Continuous Chromatography Integrated into Continuous Manufacturing of Biologics towards Autonomous Operation. *Processes* **2021**, *9*, 472. [CrossRef]
28. Uhl, A.; Schmidt, A.; Hlawitschka, M.W.; Strube, J. Autonomous Liquid–Liquid Extraction Operation in Biologics Manufacturing with Aid of a Digital Twin including Process Analytical Technology. *Processes* **2023**, *11*, 553. [CrossRef]
29. Mouellef, M.; Vetter, F.L.; Strube, J. Benefits and Limitations of Artificial Neural Networks in Process Chromatography Design and Operation. *Processes* **2023**, *11*, 1115. [CrossRef]
30. Kaczmarski, K.; Cavazzini, A.; Szabelski, P.; Zhou, D.; Liu, X.; Guiochon, G. Application of the general rate model and the generalized Maxwell–Stefan equation to the study of the mass transfer kinetics of a pair of enantiomers. *J. Chromatogr. A* **2002**, *962*, 57–67. [CrossRef] [PubMed]
31. Kaczmarski, K.; Gubernak, M.; Zhou, D.; Guiochon, G. Application of the general rate model with the Maxwell–Stefan equations for the prediction of the band profiles of the 1-indanol enantiomers. *Chem. Eng. Sci.* **2003**, *58*, 2325–2338. [CrossRef]
32. Felinger, A.; Guiochon, G. Comparison of the Kinetic Models of Linear Chromatography. *Chromatographia* **2004**, *60*, S175–S180. [CrossRef]
33. Piątkowski, W.; Antos, D.; Kaczmarski, K. Modeling of preparative chromatography processes with slow intraparticle mass transport kinetics. *J. Chromatogr. A* **2003**, *988*, 219–231. [CrossRef]
34. Asnin, L. Adsorption models in chiral chromatography. *J. Chromatogr. A* **2012**, *1269*, 3–25. [CrossRef]
35. Blümel, C.; Kniep, H.; Seidel-Morgenstern, A. Measuring adsorption isotherms using a closed-loop perturbation method to minimize sample consumption. In Proceedings of the 6th International Conference of Fundamentals of Adsorption—FOA 6, Presqu'ile de Giens, France, 23–27 May 1998; Elsevier: Amsterdam, The Netherlands, 1998; pp. 449–454.
36. Cavazzini, A.; Felinger, A.; Guiochon, G. Comparison between adsorption isotherm determination techniques and overloaded band profiles on four batches of monolithic columns. *J. Chromatogr. A* **2003**, *1012*, 139–149. [CrossRef]
37. Ching, C.B.; Chu, K.H.; Ruthven, D.M. A study of multicomponent adsorption equilibria by liquid chromatography. *AIChE J.* **1990**, *36*, 275–281. [CrossRef]
38. Gamba, G.; Rota, R.; Storti, G.; Carra, S.; Morbidelli, M. Absorbed solution theory models for multicomponent adsorption equilibria. *AIChE J.* **1989**, *35*, 959–966. [CrossRef]
39. Hu, X.; Do, D.D. Comparing various multicomponent adsorption equilibrium models. *AIChE J.* **1995**, *41*, 1585–1592. [CrossRef]
40. Heinonen, J.; Rubiera Landa, H.O.; Sainio, T.; Seidel-Morgenstern, A. Use of Adsorbed Solution theory to model competitive and co-operative sorption on elastic ion exchange resins. *Sep. Purif. Technol.* **2012**, *95*, 235–247. [CrossRef]
41. Emerton, D.A. Profitability in the Biosimilars Market: Can You Translate Scientific Excellence into a Healthy Commercial Return? *BioProcess Int.* **2013**, *11*, 6–23.
42. Erto, A.; Lancia, A.; Musmarra, D. A modelling analysis of PCE/TCE mixture adsorption based on Ideal Adsorbed Solution Theory. *Sep. Purif. Technol.* **2011**, *80*, 140–147. [CrossRef]
43. Myers, A.L.; Prausnitz, J.M. Thermodynamics of mixed-gas adsorption. *AIChE J.* **1965**, *11*, 121–127. [CrossRef]
44. Costa, E.; Calleja, G.; Marron, C.; Jimenez, A.; Pau, J. Equilibrium adsorption of methane, ethane, ethylene, and propylene and their mixtures on activated carbon. *J. Chem. Eng. Data* **1989**, *34*, 156–160. [CrossRef]
45. Brooks, C.A.; Cramer, S.M. Steric mass-action ion exchange: Displacement profiles and induced salt gradients. *AIChE J.* **1992**, *38*, 1969–1978. [CrossRef]
46. Langmuir, I. The adsorption of gases on plane surfaces of glass, mica and platinum. *J. Am. Chem. Soc.* **1918**, *40*, 1361–1403. [CrossRef]